

ORIGINAL ARTICLE

DDX17-regulated alternative splicing that produced an oncogenic isoform of PXN-AS1 to promote HCC metastasis

Hong-Zhong Zhou^{1,2} | Fan Li³ | Sheng-Tao Cheng¹ | Yong Xu² | Hai-Jun Deng¹ | Da-Yong Gu² | Jin Wang² | Wei-Xian Chen⁴ | Yu-Jiao Zhou¹ | Min-Li Yang¹ | Ji-Hua Ren¹ | Lu Zheng⁵ | Ai-Long Huang¹ | Juan Chen¹

¹The Key Laboratory of Molecular Biology of Infectious Diseases designated by the Chinese Ministry of Education, Chongqing Medical University, Chongqing, China

²Department of Clinical Laboratory, Institute of Translational Medicine, The First Affiliated Hospital of Shenzhen University, Shenzhen Second People's Hospital, Shenzhen, China

³Department of Endocrine and Breast Surgery, The First Affiliated Hospital of Chongqing Medical University, Chongqing, China

⁴Department of Clinical Laboratory, The Second Affiliated Hospital of Chongqing Medical University, Chongqing, China

⁵Department of Hepatobiliary Surgery, the Second Affiliated Hospital of Army Medical University, Chongqing, China

Correspondence

Ai-Long Huang and Juan Chen, The Key Laboratory of Molecular Biology of Infectious Diseases designated by the Chinese Ministry of Education, Chongqing Medical University, Room 617, College of Life Sciences Building, 1 Yixue Yuan Road, Yuzhong District, Chongqing, 400016, China.

Email: ahuang1964@163.com and chenjuan2014@cqmu.edu.cn

Lu Zheng, Department of Hepatobiliary Surgery, the Second Affiliated Hospital of Army Medical University, No. 183 Xinqiao High Street, Shapingba District, Chongqing, 400037, China. Email: xqyzl1@163.com

Funding information

National Natural Science Foundation of China (81861168035, 81922011, and 81871656), Creative Research Group of CQ University (CXQT19016), and Chongqing Natural Science Foundation (cstc2018jcyjAX0114)

Abstract

Background and Aims: The mechanism underlying HCC metastasis remains unclear, many oncogenes are known to regulate this process. However, the role of alternative splicing (AS) in pro-metastatic HCC is poorly understood.

Approach and Results: By performing RNA sequencing on nine pairs of primary HCC tissues with extrahepatic metastasis (EHMH) and nine pairs of metastasis-free HCC (MFH) tissues, we depicted the AS landscape in HCC and found a higher frequency of AS events in EHMH compared with MFH. Moreover, 28 differentially expressed splicing regulators were identified in EHMH compared with MFH. Among these, DEAD-box RNA helicase 17 (DDX17) was significantly up-regulated in EHMH and was strongly associated with patient outcome. Functional studies indicated that DDX17 knockout inhibited the degradation of the extracellular matrix, and diminished the invasive ability of HCC cells. A significant reduction in lung metastasis induced by DDX17 deficiency was also demonstrated in a diethylnitrosamine-induced

Abbreviations: A3SS, alternative 3' splice sites; A5SS, alternative 5' splice sites; AAV8, adeno-associated virus 8; AMPK, Adenosine Monophosphate-activated Protein Kinase; ANT, adjacent nontumor as an important promoter of HCC metastasisal tumor; AS, alternative splicing; DDX17, DEAD-box helicases 17; DEG, differentially expressed genes; DEN, diethylnitrosamine; EHMH, primary HCC tissues with extrahepatic metastasis; GSEA, gene-set enrichment analysis; IR, intron retention; lncRNA, long non-coding RNA; MFH, metastasis-free HCC tissue; MXE, mutually exclusive exon; N, nitrosodiethylamine; PIR, percent intron retention; PXN-AS1, PXN antisense transcript 1; RIP-seq, RNA immunoprecipitation sequencing; RNA-seq, RNA sequencing; SE, exon skipping; TCGA-LIHC, The Cancer Genome Atlas–Liver Hepatocellular Carcinoma; TIA1, TIA1 Cytotoxic Granule Associated RNA Binding Protein; TIAL1, TIA1 Cytotoxic Granule Associated RNA Binding Protein Like 1; Tex10, testis expressed 10.

Hong-Zhong Zhou, Fan Li, Sheng-Tao Cheng, and Yong Xu are contributed equally to this work.

This is an open access article under the terms of the Creative Commons Attribution-NonCommercial-NoDerivs License, which permits use and distribution in any medium, provided the original work is properly cited, the use is non-commercial and no modifications or adaptations are made.

© 2021 The Authors. *Hepatology* published by Wiley Periodicals LLC on behalf of American Association for the Study of Liver Diseases.

DDX17^{HKO} mouse model. Mechanistically, high DDX17 induced intron 3 retention of PXN-AS1 and produced a transcript (termed PXN-AS1-IR3). The transcript PXN-AS1-IR3 acted as an important promoter of HCC metastasis by inducing MYC transcription activation via recruiting the complex of testis expressed 10 and p300 to the MYC enhancer region, which led to transcriptional activation of several metastasis-associated downstream genes. Finally, the PXN-AS1-IR3 level was significantly higher in serum and HCC tissues with extrahepatic metastasis.

Conclusions: DDX17 and PXN-AS1-IR3 act as important metastatic promoters by modulating MYC signaling, suggesting that DDX17 and PXN-AS1-IR3 may be potential prognostic markers for metastatic HCC.

INTRODUCTION

HCC is the most common type of primary liver cancer, accounting for more than 90% of primary tumors of the liver. HCC is the second-leading cause of cancer-related death, with a low 5-year survival rate of approximately 34%–50%.^[1] The poor prognosis of HCC remains a challenge due to high rates of metastasis and postoperative recurrence.^[2,3] Therefore, a deep understanding of the mechanisms underlying HCC progression and metastasis is urgently needed.

Alternative splicing (AS) is a critical biological process for expanding gene-expression patterns and producing protein diversity.^[4] Aberrant AS events have been considered one of the critical hallmarks of cancer progression.^[5] One comprehensive analysis of the alternative splicing landscape in samples from 8705 cancer patients spanning a range of 32 cancer types revealed that tumor samples had up to 30% more AS events than normal samples.^[6] Dysregulation of splicing variants in multiple human malignancies is strongly correlated with poor differentiation, invasion and metastasis, and unfavorable prognosis.^[7] Recent studies have shown that abnormal splicing factor expression and/or activity primarily contribute to the abnormal alternative splicing patterns detected in tumors.^[8] The DEAD-box RNA helicase (DDX) family is one of the canonical splicing regulators, plays a central role in RNA metabolism, and generally functions as a part of larger multicomponent assemblies such as the spliceosome.^[9] In particular, DDX17 is gaining significant attention for its important roles in multiple pathophysiological processes. DDX17 influences cancer initiation and progression through a variety of mechanisms, such as transcriptional regulation, RNA binding, and formation of the microprocessor complex.^[10–12] More interestingly, DDX17 participates in the alternative splicing of many important tumor-related genes, such as macroH2A1 histones,^[13] Nuclear factor of activated T-cells 5 (NFAT5),^[14] and CD44.^[15] However, the role

of DDX17 in alternative splicing and HCC has not been well documented.

In this study, we reported that DDX17 was frequently up-regulated in a subset of HCC tissues and cell lines. Furthermore, we performed high-throughput RNA sequencing (RNA-seq) and identified a DDX17-modulated AS event of PXN antisense transcript 1 (lncRNA-PXN-AS1) involved in facilitating tumor metastasis of HCC. Taken together, our data demonstrate that DDX17 promotes HCC metastasis by regulating the alternative splicing of PXN-AS1, implying that DDX17 has potential as a therapeutic target for HCC therapy.

MATERIALS AND METHODS

Human samples were obtained from all patients with the written informed consent and study protocols were approved by the Ethics Committee of Chongqing medical University based on the ethical guidelines of the 1975 Declaration of Helsinki.

Cell culture

MHCC97H and Huh7 cells were cultured in Dulbecco's modified Eagle's medium supplemented with 10% fetal bovine serum (Gibco-BRL) and 1% penicillin/streptomycin. HCCLM3 cells were maintained in minimum essential medium supplemented with 10% fetal bovine serum and 1% penicillin/streptomycin. The human cell lines have been authenticated by short tandem repeat profiling within 6 months of the last experiment.

Animal experimentation

In studies involving animal experimentation, assurance was provided that all animals received humane care according to the criteria outlined in the *Guide for the*

Care and Use of Laboratory Animals. Additional methods are provided in the Supporting Information.

RESULTS

Identification of DDX17, which is an important regulator of alternative splicing, as an up-regulated gene closely associated with HCC metastasis

To broadly investigate the potential function of AS events involved in HCC metastasis, we first performed RNA-seq in nine pairs of primary HCC tissues with extrahepatic metastasis (EHMH) and nine pairs of metastasis-free HCC (MFH) tissues. Collectively, 137,402 transcripts were detected to express in the liver transcriptome, which were categorized into five types of genes (Figure S1A,B). A total of 5149 differentially expressed protein-coding genes were found in EHMH compared with paired adjacent nontumoral (ANT) tissues, whereas 4087 differentially expressed protein-coding genes were found in MFH compared with ANT (Figure S1C,D). Among these differentially expressed protein-coding genes, 38.7% (1994 of 5149) of genes in EHMH and 35.9% (1471 of 4087) of genes in MFH were transcribed into two or more dominantly expressed isoforms (Figure S1E).

Given that AS is a major contributor to this transcriptional diversity, we next analyzed AS events from the assembled transcriptomic data between EHMH and MFH. In total, we identified differentially 99,407 AS events in EHMH and 96,214 in MFH compared with ANT tissues, respectively, which can be categorized into five main AS patterns, including alternative 3' and 5' splice sites (A3SS and A5SS), mutually exclusive exons (MXE), intron retention (IR), and exon skipping (SE). The number of differentially spliced events in each EHMH and MFH were shown in Figure 1A. As expected, protein-coding genes showed the greatest number of differentially splicing events. We then evaluated the significant splicing changes of protein-coding genes and identified 1070 differentially AS events in EHMH compared with MFH. EHMH showed increased differentially splicing events relative to MFH (Figure 1B). Enrichment analysis of 798 genes that harbor 1070 differential AS events showed enrichment of many cancer metastasis-related pathways, with the top-ranked pathway highlighting regulation of actin cytoskeleton, adenosine monophosphate-activated protein kinase signaling, NF- κ B signaling, and adherens junction (Figure 1C). Moreover, we examined the splicing patterns of 1938 metastasis-associated genes from the Human Cancer Metastasis database in more detail (Table S1). A total of 140 differentially expressed metastasis-associated genes were found in EHMH compared with MFH, and 70 (70 of 140, 50.00%) genes had significant differentially AS events (Figure 1D,E). EHMH showed more significant differentially spliced events on

metastasis-associated genes with preferential increase in A3SS ($p = 0.027$), A5SS ($p = 0.041$), IR ($p = 0.029$), and SE ($p = 0.001$) (Figure 1F). These data suggest that splicing of these genes might represent an alternate mechanism for HCC metastasis.

Splicing regulators play a pivotal role in regulating the alternative splicing process.^[16] To identify dysregulated splicing regulators related to HCC metastasis, we aggregated a comprehensive list of 452 splicing regulators from different sources, including the spliceAid2 database,^[17] previous publications by Ameer et al.,^[18] Genov et al.,^[19] Sveen et al.,^[20] and Sebestyén et al.^[21] (Table S2). A total of 28 genes encoding splicing regulators were found dysregulated in EHMH compared with MFH, of which 27 genes were up-regulated and one gene was down-regulated. Of the 27 up-regulated genes, DDX17 ranks at first according to its false discovery rate (FDR) value (Figure 1G). The correlation networks between splicing regulators and AS events showed that 28 splicing regulators regulated 375 differential ASEs that were involved in many biological pathways (Figure 1H,I). Among these splicing regulators, TIA1 Cytotoxic Granule Associated RNA Binding Protein (TIA1), DDX17, and TIA1 Cytotoxic Granule Associated RNA Binding Protein Like 1 (TIAL1) regulated the greatest number of differential ASEs and involved pathways. Additionally, we analyzed the mRNA levels of these three genes in HCC samples based on The Cancer Genome Atlas–Liver Hepatocellular Carcinoma (TCGA-LIHC) database. The mRNA levels of TIA1, DDX17, and TIAL1 were significantly up-regulated in HCC tissues (Figures 2A and S1F). High expression of TIA1 and DDX17 were correlated with poor overall survival of patients with HCC, respectively, whereas no significant association of TIAL1 expression and overall survival was observed (Figures 2B and S1G). A functional experiment further revealed DDX17 knockdown exhibited the greatest inhibitory effect on the migration of HCC cells (Figure S1H).

To estimate the contribution of DDX17 to AS events underlying HCC metastasis, we used RNA-seq data sets from EHMH and MFH, and MHCC97H cells with or without DDX17 knockout, to analyze AS events. When analyzing differential AS events, we found significant overlaps of some genes in both sets of data (Figure S1I). A total of 11.3% (8 of 71) of genes with IR, 9.3% (52 of 557) of genes with SE, 6.3% (8 of 126) of genes with A3SS, 4.5% (3 of 66) genes with MXE, and 2.3% genes (2 of 88) with A5SS in EHMH were DDX17-related. These data suggest the important role of DDX17 in HCC metastasis. Therefore, we focused on the functional roles and related mechanisms of DDX17 in driving HCC metastasis.

High level of DDX17 correlates with poor prognosis of HCC patient

Next, we aimed to reveal the clinical significance of DDX17 in HCC. As mentioned previously, high

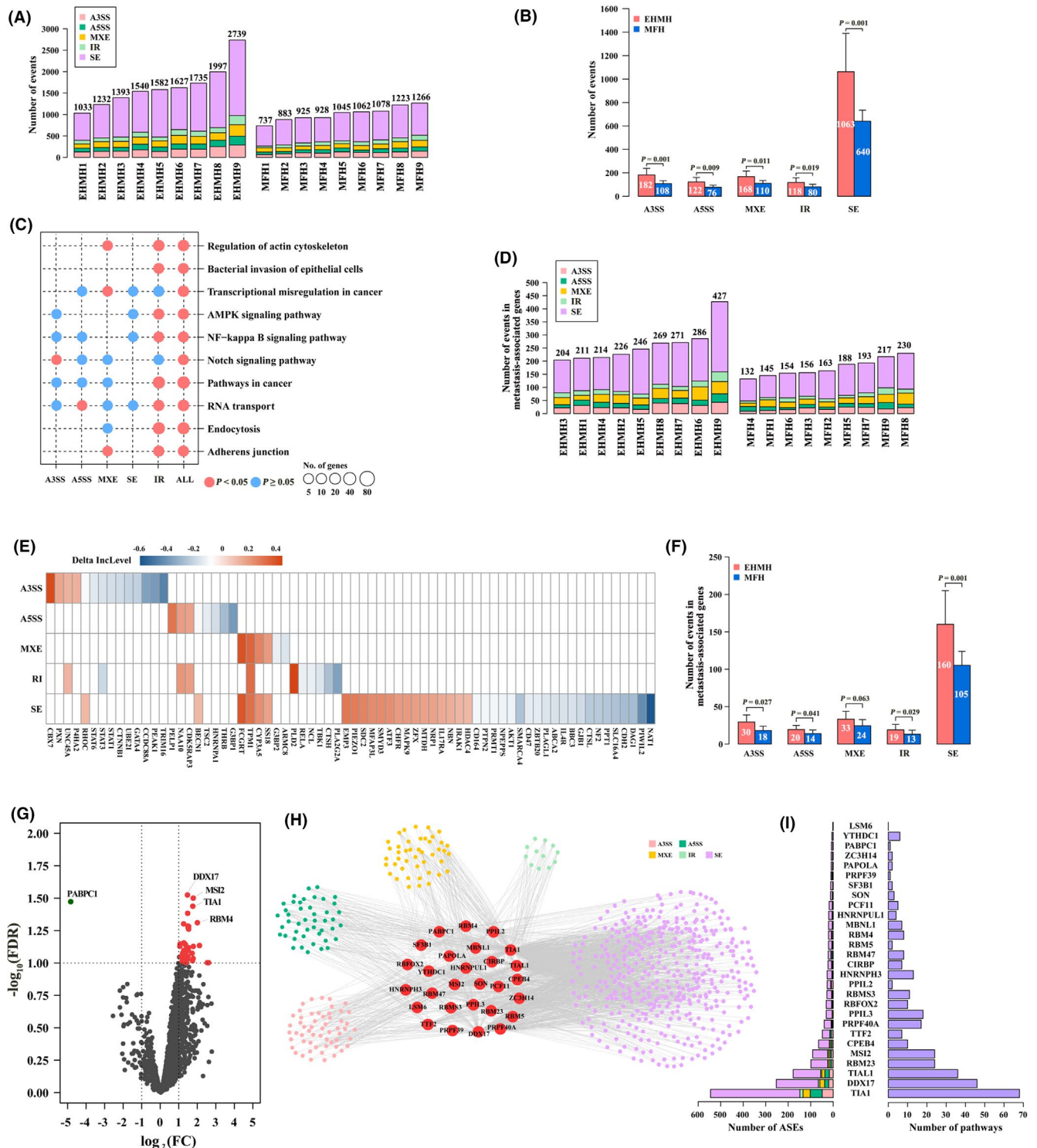


FIGURE 1 Legend on next page

expression of DDX17 in HCC samples was found in the TCGA-LIHC data sets, which was strongly associated with patient poor outcome (Figure 2A,B). Among 371 patients in the TCGA-LIHC data sets, 93 patients with no information of American Joint Committee on Cancer (AJCC) Tumor Node Metastasis stage, tumor histological grade, HBV, macroscopic vascular invasion, and microscopic vascular invasion were

excluded. Correlative analysis suggested significant association between increased DDX17 expression and sex ($p < 0.0001$), tumor histological grade ($p = 0.0031$), alpha-fetoprotein (AFP; $p = 0.001$), and vascular invasion ($p = 0.0452$) (Table S3). Consistently, GSE14520 data sets revealed that DDX17 was more highly expressed in HCCs than that in nontumoral tissues (Figure S2A).

FIGURE 1 Identification of DEAD-box RNA helicase 17 (DDX17) as an up-regulated gene closely associated with HCC metastasis. (A) The number of differentially splicing events between HCC and paired adjacent nontumor tissues (ANT) in patients with HCC with extrahepatic metastasis (EHMH) or metastasis-free (MFH). The differentially expressed gene (DEG) analysis between paired primary tumor and ANT was performed by R package edgeR, and differentially AS events analysis was performed by rMarts. The numbers of differentially splicing events between paired primary tumor and ANT are indicated. (B) Comparison of differentially splicing events in five types of alternative splicing (AS) events between EHMH and MFH. The numbers in the bars represent the average number of differentially spliced events between nine paired HCC tissues and ANT. (C) Pathway enrichment analysis for 798 genes that harbor 1070 differential Alternative Splicing Events (ASEs). $p < 0.05$ was considered statistically significant. (D) The number of events in metastasis-associated genes between EHMH and MFH. The numbers of differentially metastasis-associated ASEs between paired primary tumor and adjacent non-tumor tissue are indicated. (E) Detailed splicing event information of 70 metastasis-associated genes in each EHMH and MFH. (F) Comparison of differentially splicing events of metastasis-associated genes in five types of AS events between EHMH and MFH. The average numbers of differentially splicing events in EHMH and MFH group are indicated. (G) Volcano plot of 452 splicing regulators between EHMH and MFH tissues. Each gene is plotted according to its expression level (\log_2FC) and false discovery rate (FDR) value ($-\log_{10}[FDR]$). Red indicates up-regulated. Green indicates down-regulated. (H) The correlation network between the mRNA levels of 28 splicing regulators and Inclusion Level (IncLevel) of differentially splicing events in the EHMH and MFH. The correlation analysis was performed by using Pearson correlation analysis ($|Pearson\ correlation| > 0.7$, $\Delta|Inclevel| > 0.1$, and $p < 0.05$ were considered statistically significant. (I) Number of ASEs and pathways regulated by splicing regulators. The left panel indicates the number of differential ASEs regulated by each splicing regulator ($|Pearson\ correlation| > 0.7$ and $p < 0.05$). The right panel shows the number of pathways regulated by splicing regulators ($p < 0.05$). For differentially expressed gene (DEG) analysis, $|\log_2FC| > 2$ and $p < 0.05$ were considered statistically significant. For differential ASE analysis, $|\Delta\ Inclevel| > 0.1$ and $p < 0.05$ were considered statistically significant. A3SS, alternative 3' splicing site; A5SS, alternative 5' splicing site; ABCA2, ATP Binding Cassette Subfamily A Member 2; AKT1, AKT Serine/Threonine Kinase 1; AMPK, adenosine monophosphate-activated protein kinase; ARMC8, Armadillo Repeat Containing 8; ATF3, Activating Transcription Factor 3; BBC3, BCL2 Binding Component 3; BECN1, Beclin 1; CBX7, Chromobox 7; CCDC88A, Coiled-Coil Domain Containing 88A; CD164, CD164 Molecule; CD47, CD47 Molecule; CDH2, Cadherin 2; CDK5RAP3, CDK5 Regulatory Subunit Associated Protein 3; CHFR, Checkpoint With Forkhead And Ring Finger Domains; CIRBP, Cold Inducible RNA Binding Protein; CPEB4, cytoplasmic Polyadenylation Element Binding Protein 4; CTNNB1, Catenin Beta 1; CTSH, Cathepsin H; CTSL, Cathepsin L; CYP3A5, Cytochrome P450 Family 3 Subfamily A Member 5; DAG1, Dystroglycan 1; EMP3, Epithelial Membrane Protein 3; FCGRT, Fc Fragment Of IgG Receptor And Transporter; G3BP1, G3BP Stress Granule Assembly Factor 1; G3BP2, G3BP Stress Granule Assembly Factor 2; GATA4, GATA Binding Protein 4; GJB1, Gap Junction Protein Beta 1; HNRNPA1, Heterogeneous Nuclear Ribonucleoprotein A1; HNRNPH3, Heterogeneous Nuclear Ribonucleoprotein H3; HNRNPUL1, Heterogeneous Nuclear Ribonucleoprotein U Like 1; IL17RA, Interleukin 17 Receptor A; IL4R, Interleukin 4 Receptor; IR, intron retention; IRAK1, Interleukin 1 Receptor Associated Kinase 1; HDAC4, Histone Deacetylase 4; LSM6, LSM6 Homolog, U6 Small Nuclear RNA And mRNA Degradation Associated; MAPK9, Mitogen-Activated Protein Kinase 9; MBNL1, Muscblind Like Splicing Regulator 1; MFAP3L, Microfibril Associated Protein 3 Like; MSI2, Musashi RNA Binding Protein 2; MTDH, Metadherin; MXE, mutually exclusive exon; NAA10, N-Alpha-Acetyltransferase 10, NatA Catalytic Subunit; NAT1, N-Acetyltransferase 1; NBN, Nibrin; NCL, Nucleolin; NF2, Neurofibromin 2; NPEPPS, Aminopeptidase Puromycin Sensitive; NRP1, Neuropilin 1; P4HA2, Prolyl 4-Hydroxylase Subunit Alpha 2; PABPC1, Poly(A) Binding Protein Cytoplasmic 1; PAPOLA, Poly(A) Polymerase Alpha; PCF11, PCF11 Cleavage And Polyadenylation Factor Subunit; PEAK1, Pseudopodium Enriched Atypical Kinase 1; PELP1, Proline, Glutamate And Leucine Rich Protein 1; PIEZO1, Piezo Type Mechanosensitive Ion Channel Component 1; PIWIL2, Piwi Like RNA-Mediated Gene Silencing 2; PLA2G2A, Phospholipase A2 Group IIA; PLAGL1, PLAG1 Like Zinc Finger 1; PLD2, Phospholipase D2; PPLI2, Peptidylprolyl Isomerase Like 2; PPLI3, Peptidylprolyl Isomerase Like 3; PPT1, Palmitoyl-Protein Thioesterase 1; PRMT1, Protein Arginine Methyltransferase 1; PRPF39, Pre-mRNA Processing Factor 39; PRPF40A, Pre-mRNA Processing Factor 40 Homolog A; PTPN2, Protein Tyrosine Phosphatase Non-Receptor Type 2; PXN, Paxillin; RBFox2, RNA Binding Fox-1 Homolog 2; RBM23, RNA Binding Motif Protein 23; RBM4, RNA Binding Motif Protein 4; RBM47, RNA Binding Motif Protein 47; RBM5, RNA Binding Motif Protein 5; RBMS3, RNA Binding Motif Single Stranded Interacting Protein 3; RELA, RELA Proto-Oncogene, NF-KB Subunit; RHOC, Ras Homolog Family Member C; SDC2, Syndecan 2; SE, skipping exon; SF3B1, Splicing Factor 3b Subunit 1; SLC16A4, Solute Carrier Family 16 Member 4; SMARCA4, SWI/SNF Related, Matrix Associated, Actin Dependent Regulator Of Chromatin, Subfamily A, Member 4; SMYD3, SET And MYND Domain Containing 3; SON, SON DNA And RNA Binding Protein; SS18, SS18, Subunit Of BAF Chromatin Remodeling Complex; STAT1, Signal Transducer And Activator Of Transcription 1; STAT3, Signal Transducer And Activator Of Transcription 3; STAT6, Signal Transducer And Activator Of Transcription 6; TBK1, TANK Binding Kinase 1; THRB, Thyroid Hormone Receptor Beta; TPM1, Tropomyosin 1; TRIM16, Tripartite Motif Containing 16; TSC2, TSC, Complex Subunit 2; TTF2, Transcription Termination Factor 2; UBE2L, Ubiquitin Conjugating Enzyme E2 L; UNC45A, Unc-45 Myosin Chaperone A; YTHDC1, YTH Domain Containing 1; ZBTB20, Zinc Finger And BTB Domain Containing 20; ZC3H14, Zinc Finger CCCH-Type Containing 14; ZFX, Zinc Finger Protein X-Linked

To further establish the relevance of DDX17 expression in HCC, we determined DDX17 expression in 84 pairs of primary HCC and adjacent nontumoral liver tissues collected in our laboratory using quantitative real-time PCR. We found that mRNA level of *DDX17* was significantly increased in HCCs compared with those in adjacent nontumoral liver tissues (Figure 2C,D). The expression level of *DDX17* in HCC tissues was inversely correlated with the overall survival of patients with HCC (Figure 2E). Univariate analysis also indicated that high expression of *DDX17* was significantly associated

with AFP ($p = 0.035$), tumor size ($p = 0.0151$), tumor grade ($p = 0.007$), and vascular invasion ($p = 0.037$) (Table S4). To further explore the role of DDX17 in HCC metastasis, both the mRNA and protein levels of DDX17 were examined in 28 HCCs with metastasis and 56 metastasis-free HCCs. Consistently, elevated expression of DDX17 was found in metastatic HCC tissues compared with metastasis-free HCC tissues (Figures 2F–H and S2B). Taken together, these data suggest that DDX17 overexpression is significantly associated with poor prognosis of HCC.

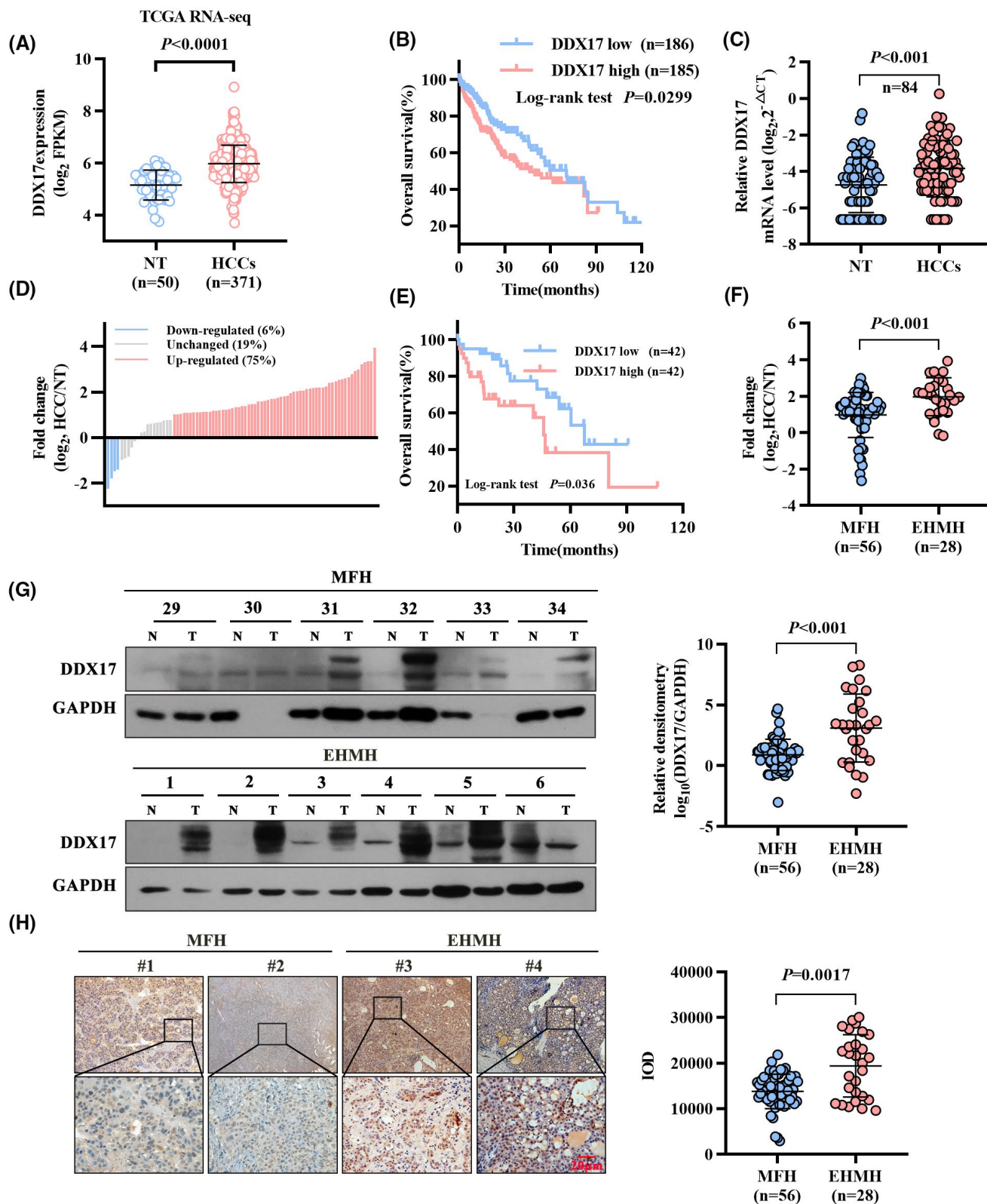


FIGURE 2 Legend on next page

DDX17 promotes HCC growth and metastasis

To ascertain the function of DDX17 in HCC cells, endogenous DDX17 was stably knocked out in

MHCC97H and HCCLM3 cells, which have higher invasive and metastatic capabilities, by using the CRISPR/Cas9 system (Figure S3A–D). DDX17 knock-out resulted in a considerable inhibitory effect on proliferation and colony-forming abilities of HCC cells, as

FIGURE 2 Up-regulation of DDX17 in patients with HCC is closely related to clinical survival. (A) The mRNA level of DDX17 in HCC samples ($n = 371$) and nontumoral tissues ($n = 50$) was determined by analyzing RNA-seq data from the TCGA-LIHC database ($p < 0.0001$). (B) Kaplan-Meier survival analysis for the correlation between DDX17 mRNA level and overall survival in patients with HCC from The Cancer Genome Atlas–Liver Hepatocellular Carcinoma (TCGA-LIHC) cohort (log-rank test, $p = 0.029$). (C,D) DDX17 mRNA level was detected in 84 paired HCC tissues and adjacent nontumoral (NT) liver tissues by quantitative real-time PCR. (E) Kaplan-Meier survival analysis for the correlation between DDX17 mRNA level and overall survival in 84 paired HCC tissues and ANT liver tissues. (F) Real-time PCR was performed to determine the mRNA level of DDX17 in primary HCC tissues with EHMH and MFH tissues. (G) Western blot was used to detect DDX17 protein level in primary HCC tissues with EHMH and MFH tissues; the band intensity was calculated by Image J software. GAPDH was used as loading control. (H) Immunohistochemistry was used to examine the expression of DDX17 in EHMH ($n = 28$) or MFH ($n = 56$); the expression level was calculated by Image J software. Scar bars, 20 μm . GAPDH, glyceraldehyde 3-phosphate dehydrogenase; N, non-tumor adjacent tissues; T, tumor

evidenced by trypan blue dye–positive cell counts and soft agar assays (Figure S3E,F). In contrast, ectopic expression of DDX17 exhibited the opposite effects in Huh-7 cells, which have low metastatic potential (Figure S3G-I). Moreover, DDX17 knockout diminished the wound-healing capacity and significantly inhibited the migration and invasion of MHCC97H and HCCLM3 cells (Figures 3A and S4A), whereas overexpression of DDX17 enhanced the migration and invasion of Huh-7 cells (Figure S4B,C). Invadopodia are actin-rich membrane protrusions that degrade the surrounding extracellular matrix for invasion. Therefore, the effect of DDX17 knockout on invadopodia function was tested by gelatin degradation assay in MHCC97H and HCCLM3 cells. The function of invadopodia was judged by co-localizing the actin cytoskeleton and nuclei with fluorescent gelatin degradation sites. DDX17 knockout diminished the invasive ability of MHCC97H and HCCLM3 cells, as evidenced by decreased areas devoid of fluorescence where the cell has degraded the matrix (Figures 3B and S4D). Lamellipodia is a dynamic surface extension of the cell, which plays a pivotal role in cell migration. F-actin staining revealed that lamellipodia formation was markedly decreased in MHCC97H and HCCLM3 cells after DDX17 was knocked out (Figures 3C and S4E).

To confirm these findings, we further examined the effect of DDX17 knockout on tumor growth and metastasis of HCC cells *in vivo*. Hepatocyte-specific DDX17 knockout mice (DDX17^{HKO}) were established by crossing DDX17^{fl/fl} mice with Alb-Cre mice (Figure S5A–C). In the diethylnitrosamine (DEN)/CCl₄-induced hepatocarcinogenesis model, in which DDX17^{fl/fl} and DDX17^{HKO} mice were injected intraperitoneally with either DEN or CCl₄, we regularly sacrificed one cohort of mice every 2 months after 8 months of DEN injection to monitor the development of HCC. The decreased incidence of liver tumors was observed in DDX17^{HKO} mice compared with that of DDX17^{fl/fl} mice. Liver tumors were detected in 89% (8 of 9) of the control DDX17^{fl/fl} mice, whereas macroscopic observations revealed that approximately 30% of DDX17^{HKO} mice developed liver tumors 14 months after DEN treatment (Table S5). Importantly, dramatic decrease in the number and size of liver tumors as well as lung metastasis foci were found in DDX17^{HKO} mice (Figure 3D,E). About

70%–80% of the DDX17^{fl/fl} mice developed lung metastases, whereas only 20%–30% of the DDX17^{HKO} mice had lung metastasis (Table S6). Moreover, we injected the stable DDX17-overexpressing HCC cells into the left lobe of orthotopic liver to establish a mouse model of lung metastasis. Overexpression of DDX17 significantly promoted the liver tumor volume and number (Figures 3F and S5D), as well as the number of lung metastatic nodules and foci (Figure 3G). Collectively, these *in vitro* and *in vivo* gain-of-function and loss-of-function studies suggest that DDX17 plays important roles in promoting HCC growth and metastasis.

DDX17 induces lncRNA-PXN-AS1 intron 3 retention in HCC cells

To elucidate the molecular mechanism of DDX17 in promoting HCC metastasis, we analyzed the AS events regulated by DDX17 in MHCC97H cells with or without DDX17 knockout by using RNA-seq. A total of DDX17-regulated 7582 AS events in 2807 long non-coding RNAs (lncRNAs) and 47,943 AS events in 11,627 mRNAs with significant changes were identified. We then performed RNA immunoprecipitation sequencing (RIP-seq) and identified 220 DDX17-associated lncRNAs and 2048 mRNAs in MHCC97H cells (Figure S6A). Combining the RIP-seq data and the RNA-seq data, we found 17 closely DDX17-associated lncRNAs (17 of 220, 7.73%) and 107 DDX17-associated mRNAs (107 of 2048, 5.22%) with differential AS events (Figure 4A and Table S7). Among these DDX17-related lncRNAs (10 lncRNAs annotated, 7 lncRNAs novel), 50.0% (5 of 10) of annotated lncRNAs were involved in cancer metastasis, whereas only 13.1% (14 of 107) of genes were closely related to cancer metastasis (Table S8). These data suggest that DDX17 might show preference for influencing lncRNA to drive metastasis of HCC. Among the most significant AS events of lncRNAs, we noted the regulation of alternative splicing events, which included 40% SE, 26% IR, 17% A5SS, 14% alternative 3' splicing site A3SS, and 3% mutually exclusive exon MXE (Figure 4B).

Next, we searched for lncRNA that might participate in DDX17-mediated growth and metastasis of HCC cells. To evaluate the accuracy of our RNA-seq

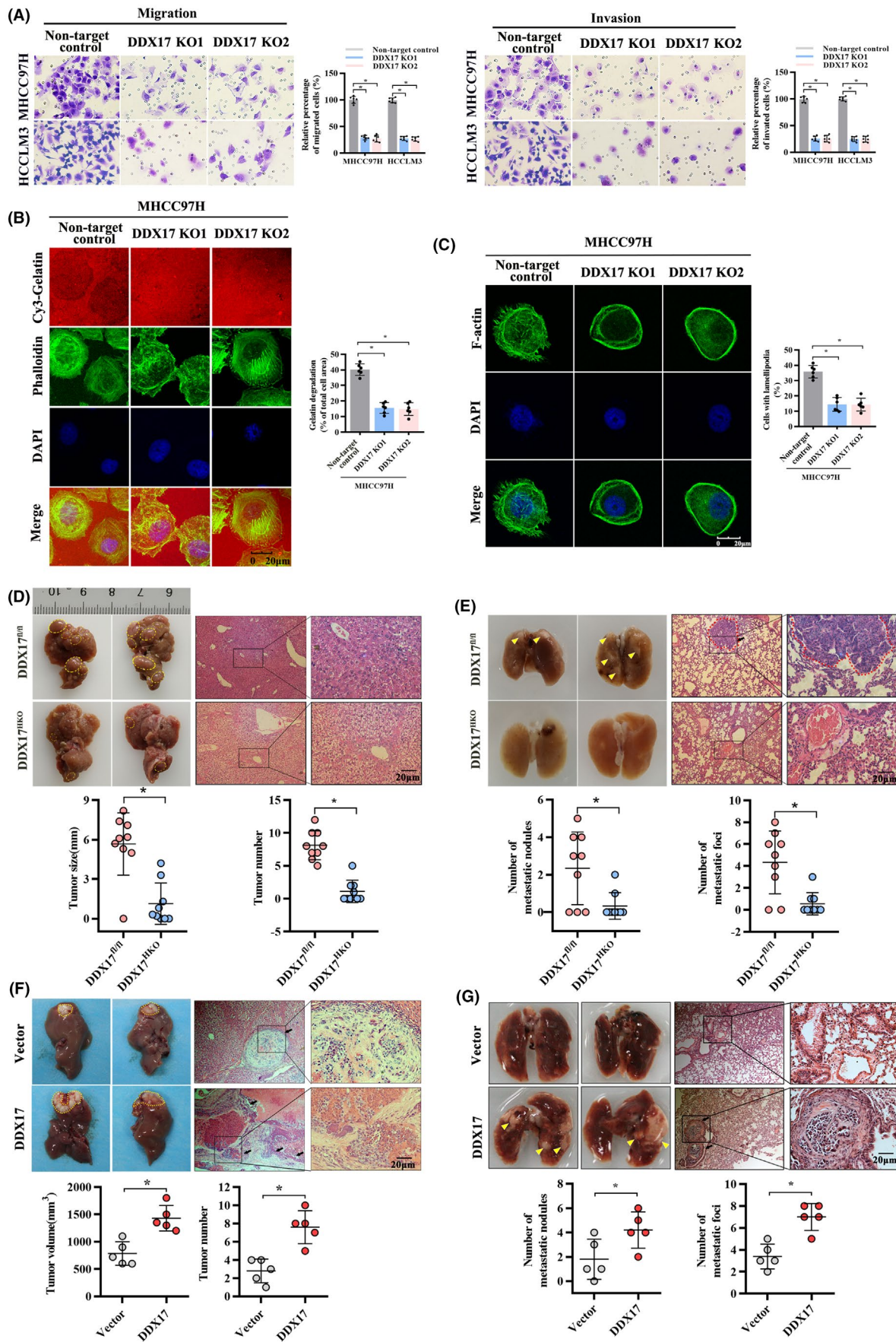


FIGURE 3 Legend on next page

FIGURE 3 DDX17 knockout inhibits HCC metastasis in vitro and in vivo. (A) Effect of DDX17 knockout on migration and invasion of MHCC97H and HCCLM3 cells evaluated by transwell assays. The cells were counted from six images ($*p < 0.05$). (B) Effect of DDX17 knockout on invadopodia function was tested by gelatin degradation assay in MHCC97H. Cells were plated onto Cy3-gelatin substrates (red) and cultured for 48 h. Following staining with fluorescein isothiocyanate-phalloidin (green) and 4',6-diamidino-2-phenylindole (DAPI) (blue), cells were imaged using confocal, and representative images are shown. The degraded areas were quantified using Image J software from at least six fields. $*p < 0.05$. Scale bar, 20 μm . (C) Lamellipodia formation was analyzed by F-actin staining in MHCC97H cells with or without DDX17 knockout. Representative images were shown. Scale bar, 20 μm . Percentage of cells with lamellipodia formation were counted. $*p < 0.05$. (D,E) DEN/ CCl_4 -induced hepatocarcinogenesis model were established in hepatocyte-specific DDX17 knockout mice (DDX17^{HKO}) and corresponding control mice (DDX17^{fl/fl}). Liver and lung were collected at 14 months following DEN treatment, which was further subjected to hematoxylin and eosin (H&E) staining ($n = 9$). (D) Representative images of tumor-bearing liver were provided and average tumor size was calculated (left); representative images of H&E staining for livers tissues were provided and tumor number was counted (right). (E) Representative images of lung were provided and metastatic nodules were counted (left); representative images of H&E staining for lung tissues were provided and metastatic foci were counted (right). $*p < 0.05$. (F,G) Huh7 cells with DDX17 stably expressed were orthotopically injected into the left lobe liver of nude mice to establish a lung metastasis model. Liver and lung were collected at 8 weeks following injection and subjected to H&E staining. (F) Representative images of tumor-bearing liver were provided and tumor volume was calculated (left); representative images of H&E staining for livers tissues were provided and tumor number was counted (right). (G) Representative images of lung were provided and metastatic nodules were counted (left); representative images of H&E staining for lung tissues were provided and metastatic foci were counted (right). $*p < 0.05$

analysis of lncRNA splicing changes, we individually measured AS events of 17 lncRNAs in DDX17 knockout cells. Finally, we focused on lncRNA-PXN-AS1, which belongs to NONCODE, Lnc2Cancer and TANRIC, and showed splicing events that changed significantly in response to DDX17 knockout (Figure S6B and Table S9). Nine PXN-AS1 splice variants (ENST00000535200.1, ENST00000538804.5, ENST00000539446.6, ENST00000542265.6, ENST00000542314.5, ENST00000620336.1, ENST00000664264.1, ENST00000667017.1, and ENST00000667721.1) were screened and found that only PXN-AS1-205 transcript was dramatically increased in DDX17 KO cells (Figure S6C). Ensemble gene database showed that the PXN-AS1-205 (ENST00000542314.5, termed PXN-AS1-WT) consists of four exons and three introns (Figure S6D). The transcript PXN-AS1-205 with intron 3 retention (termed PXN-AS1-IR3) was markedly decreased in DDX17 knockout cells, whereas PXN-AS1-IR3 was significantly up-regulated in DDX17-overexpressing cells (Figure 4C,D). Sashimi plot visualization of sequencing data validated the intron 3 retention of PXN-AS1 (Figure S6E). Moreover, the PXN-AS1 with intron 3 retention occurred in the RNA-seq of EHMH and MFH tissues (Figure 4E).

To determine whether this effect on alternative splicing was mediated by direct binding of DDX17, we performed RNA-immunoprecipitation assays and found that DDX17 immunoprecipitated RNAs containing PXN-AS1 (Figure 4F). Consistently, the association of PXN-AS1 with DDX17 was validated by RNA pulldown assays (Figure 4G). To elucidate the underlying mechanism of DDX17-mediated PXN-AS1 splicing, we constructed a minigene of PXN-AS1 genomic DNA that contained lncRNA-PXN-AS1 exon 3, intron 3, exon 4, and the flanking intronic sequences. Consistently, depletion of DDX17 repressed intron 3 retention, whereas overexpression of DDX17 induced intron 3 retention

(Figure 4H,I). Moreover, expression of the PXN-AS1-IR3 isoform was decreased in the DDX17-knockout cells, while the expression of the PXN-AS1-IR3 was increased in response to DDX17 overexpression (Figure 4J). Collectively, these data demonstrate that DDX17 regulates alternative splicing of lncRNA-PXN-AS1 by inducing intron retention in HCC cells.

PXN-AS1-IR3 promotes HCC cell migration in vitro and in vivo

We then investigated the function of different PXN-AS1 isoforms in HCC. First, the coding potential calculator and coding potential assessment tool indicated that neither PXN-AS1-IR3 nor PXN-AS1-WT have protein-coding potential (Figure S7A). The full-length sequences of PXN-AS1-IR3 in HCC cells were identified by the 5' and 3' rapid amplification of complementary DNA ends (Figure S7B). Moreover, northern blot analysis confirmed that both 858-nt PXN-AS1-IR3 and 707-nt PXN-AS1-WT were stable transcripts in HCC cells (Figure S7C). RNA fluorescent in situ hybridization assays and northern blot analysis of RNA in cytoplasmic and nuclear fractions revealed that PXN-AS1-IR3 distributed in both the nucleus and cytoplasm of MHCC97H and HCCLM3 cells (Figure S7D–F).

We analyzed the cellular gain-of-function phenotype in HCC cells to address the oncogenic function of PXN-AS1-IR3. Overexpression of PXN-AS1-IR3, but not PXN-AS1-WT, resulted in an increase in wound-healing capacity, cell migration, and invasion in vitro (Figure 5A–C). Fluorescent gelatin degradation assay showed increased activity of extracellular matrix degradation in HCC cells ectopically expressing PXN-AS1-IR3, but not PXN-AS1-WT (Figures 5D and S8A). Importantly, PXN-AS1-IR3 overexpression, but not PXN-AS1-WT, significantly enhanced hepatocarcinogenesis and lung metastasis in the orthotopic

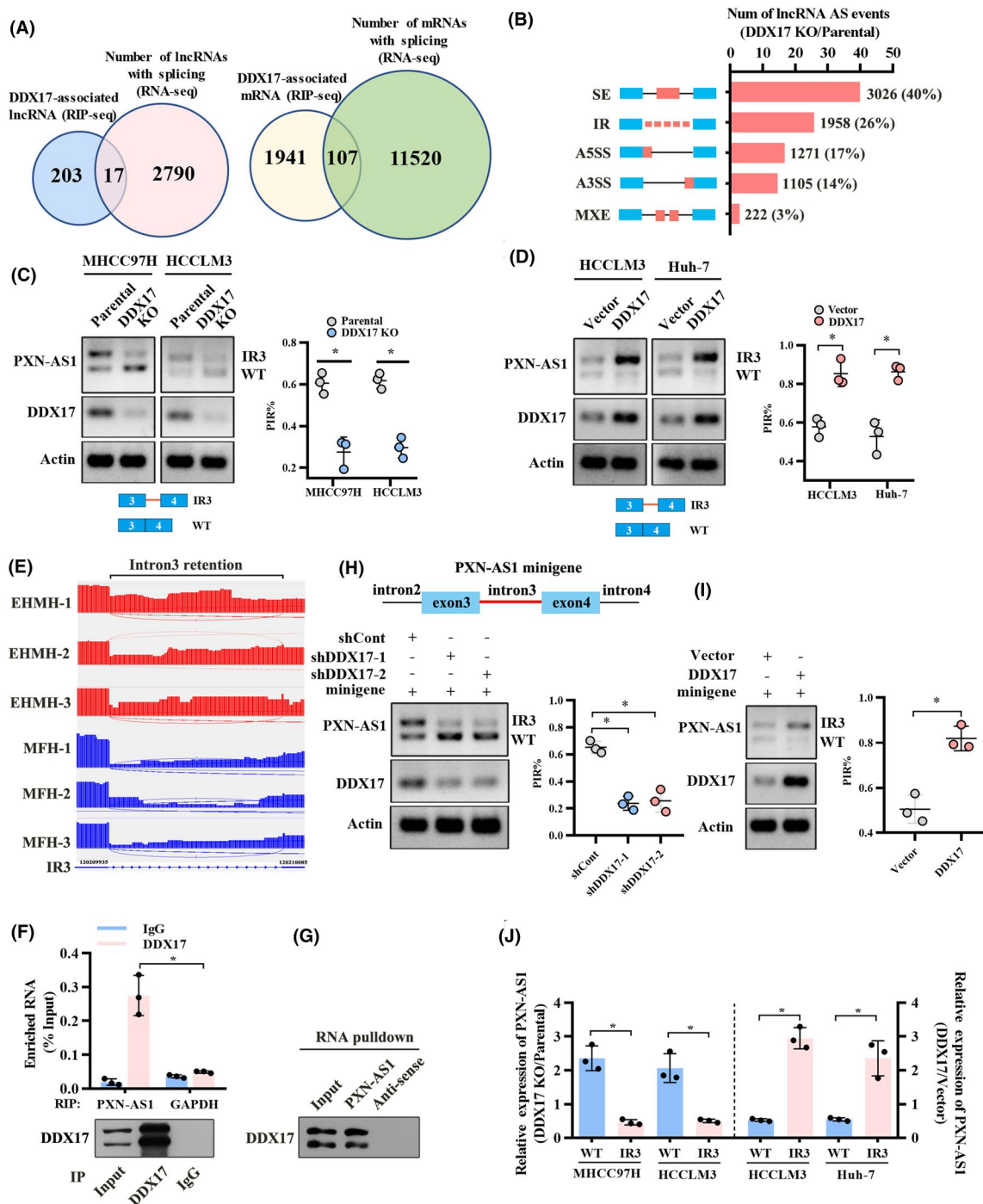


FIGURE 4 DDX17 induces long non-coding RNA (lncRNA)-PXN-AS1 intron 3 retention in HCC cells. (A) DDX17-associated lncRNA identified by RNA immunoprecipitation sequencing (RIP-seq) and DDX17-regulated downstream lncRNA splicing events determined by RNA sequencing (RNA-seq) are illustrated by Venn diagram (left); DDX17-associated mRNA identified by RIP-seq and DDX17-regulated downstream mRNA splicing events determined by RNA-seq are illustrated by Venn diagram (right). (B) lncRNA alternative splicing events regulated by DDX17 were analyzed by RNA-seq. (C,D) Intron retention (IR) of PXN-AS1 in DDX17-knockout cells (C) or DDX17-overexpression cells (D) were measured by agarose gel electrophoresis of PCR products. Gel densitometry was analyzed by Image J to calculate percent intron retention (PIR). (E) Sashimi plots illustrate RNA-seq read coverage for PXN-AS1-IR3 in EHMH (red) and MFH tissues (blue). Splicing events are highlighted by inverted brackets. Splicing events were defined based on the genomic organization of Ref-seq transcripts (bottom). (F) Enrichment of PXN-AS1 on DDX17 was detected by RIP assay (top). Western blot was performed to confirm that DDX17 was immunoprecipitated in the RIP experiments (bottom). (G) Specific association of DDX17 with biotinylated-PXN-AS1 was detected by streptavidin RNA pull-down assay. (H,I) Schematic diagram shows the design of the PXN-AS1-IR3 minigene. The effect of DDX17 knockdown (H) or overexpression (I) on AS of PXN-AS1 minigene was detected by agarose gel electrophoresis of PCR products. Gel densitometry was analyzed by Image J to calculate PIR. (J) Expression level PXN-AS1 in DDX17 knockout or stably overexpressing cells was determined by Real-time PCR. * $p < 0.05$. IP, immunoprecipitation; KO, knockout; WT, PXN-AS1-WT; IR3, PXN-AS1-IR3

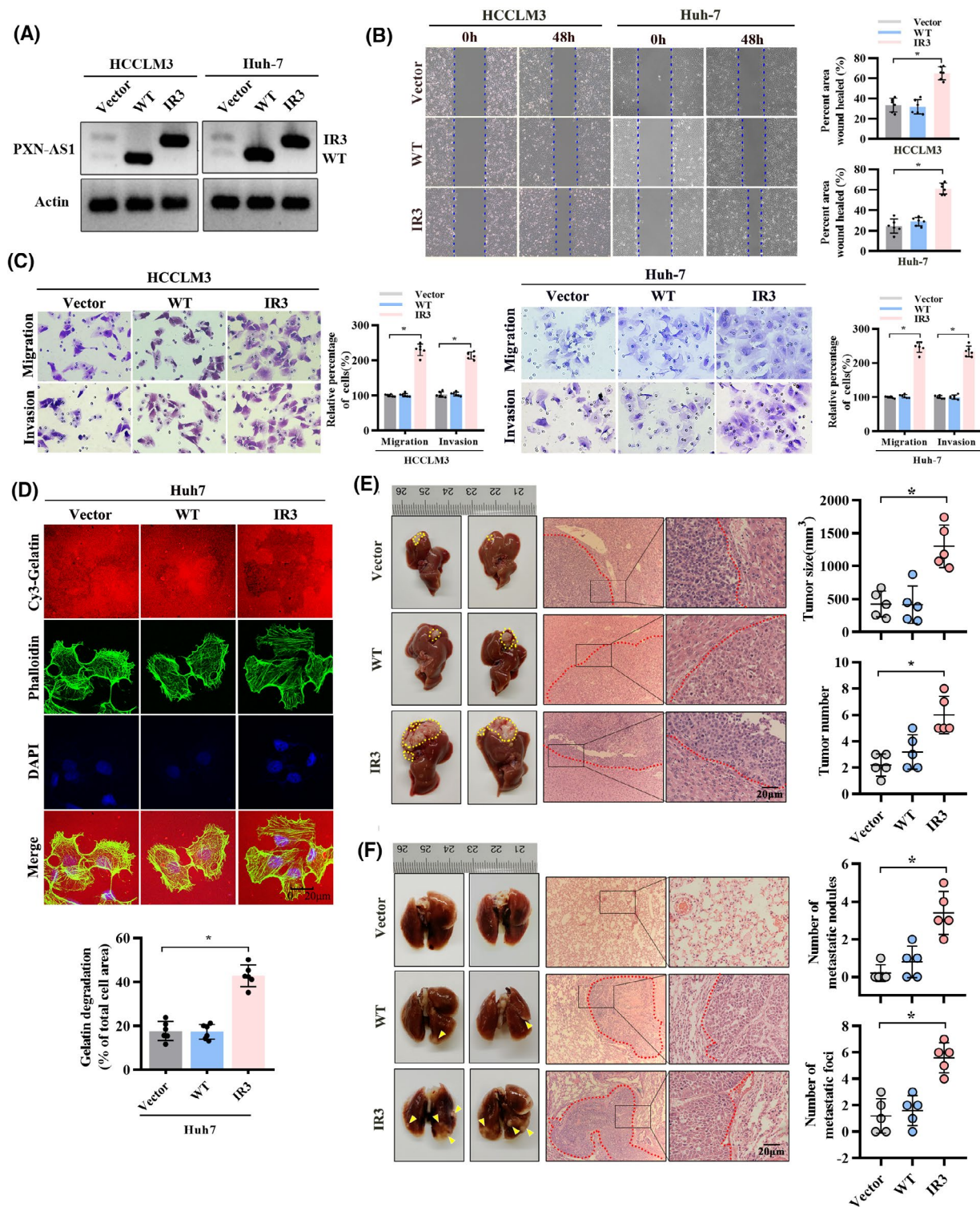


FIGURE 5 PXN-AS1-IR3 promotes HCC cell migration and invasion in vitro and in vivo. (A) Efficiency of PXN-AS1-WT and PXN-AS1-IR3 overexpression was confirmed by PCR, and the products were subjected to agarose gel electrophoresis. (B) Effect of PXN-AS1-WT and PXN-AS1-IR3 overexpression on cell migratory capacity was determined by scratch wound healing assay. The distance was measured from six images. (C) Effect of PXN-AS1-WT and PXN-AS1-IR3 overexpression on migration and invasion in vitro was determined by transwell assays. The cells were counted from six images. * $p < 0.05$. (D) Effect of PXN-AS1-WT and PXN-AS1-IR3 overexpression on invadopodia function was tested by gelatin degradation assay in Huh-7 cell. The images were captured by using confocal and representative images. The degraded areas were quantified using Image J software from six fields. Scar bars, 20 μm . * $p < 0.05$. (E,F) Huh-7 cells with PXN-AS1-IR3 or PXN-AS1-WT stably expressed were orthotopically injected into the left lobe liver of nude mice to establish a lung metastasis model. Liver and lung were collected at 8 weeks following injection and subjected to H&E staining. (E) Representative images of tumor-bearing liver and H&E staining for livers tissues were provided. Tumor size and tumor number were calculated. * $p < 0.05$. (F) Representative images of lung and H&E staining for lung tissues were provided; the metastatic nodules and metastatic foci were counted. * $p < 0.05$

nude mouse HCC model (Figure 5E,F). In contrast, we investigate the effect of PXN-AS1-IR3 knockdown on HCC metastasis. Two independent short hairpin RNAs (shIR3-1 and shIR3-2), which specifically knocked down PXN-AS1-IR3, significantly decreased the wound-healing capacity, migration, and invasion activities of HCC cells (Figure S9A–D). PXN-AS1-IR3 knockdown impaired extracellular matrix degradation (Figure S9E) and decreased lamellipodia formation in HCC cells (Figure S9F). PXN-AS1-IR3 knockdown significantly inhibited hepatocarcinogenesis and lung metastasis in the orthotopic nude mouse HCC model (Figure S10A,B). Collectively, these findings suggest that PXN-AS1-IR3 acts as an oncogenic driver in the development and progression of HCC.

To investigate whether PXN-AS1-IR3 was involved in DDX17-mediated HCC metastasis, we overexpressed PXN-AS1-IR3 in DDX17 knockout cells. DDX17 knockout significantly decreased the migration and invasion abilities of these cells. Subsequently, PXN-AS1-IR3 overexpression markedly restored the migration and invasion abilities of DDX17 knockout cells (Figure S11A,B). Next, we evaluated the pro-tumorigenic effect of PXN-AS1-IR3 on liver tumors in 12-month-old DEN-treated DDX17^{HKO} mice via tail vein injection of adeno-associated virus 8 (AAV8)–green fluorescent protein ($n = 7$) and AAV8-PXN-AS1-IR3 ($n = 8$). Reintroduction of PXN-AS1-IR3 significantly promoted the numbers and sizes of liver tumors in DDX17^{HKO} mice (Figure S11C,D). Moreover, the numbers of lung metastases in AAV8-PXN-AS1-IR3-treated mice were significantly higher than those of their counterparts DDX17^{HKO} mice (Figure S11E,F). Together, these results demonstrate that PXN-AS1-IR3 is involved in the DDX17-mediated signaling pathway of HCC migration.

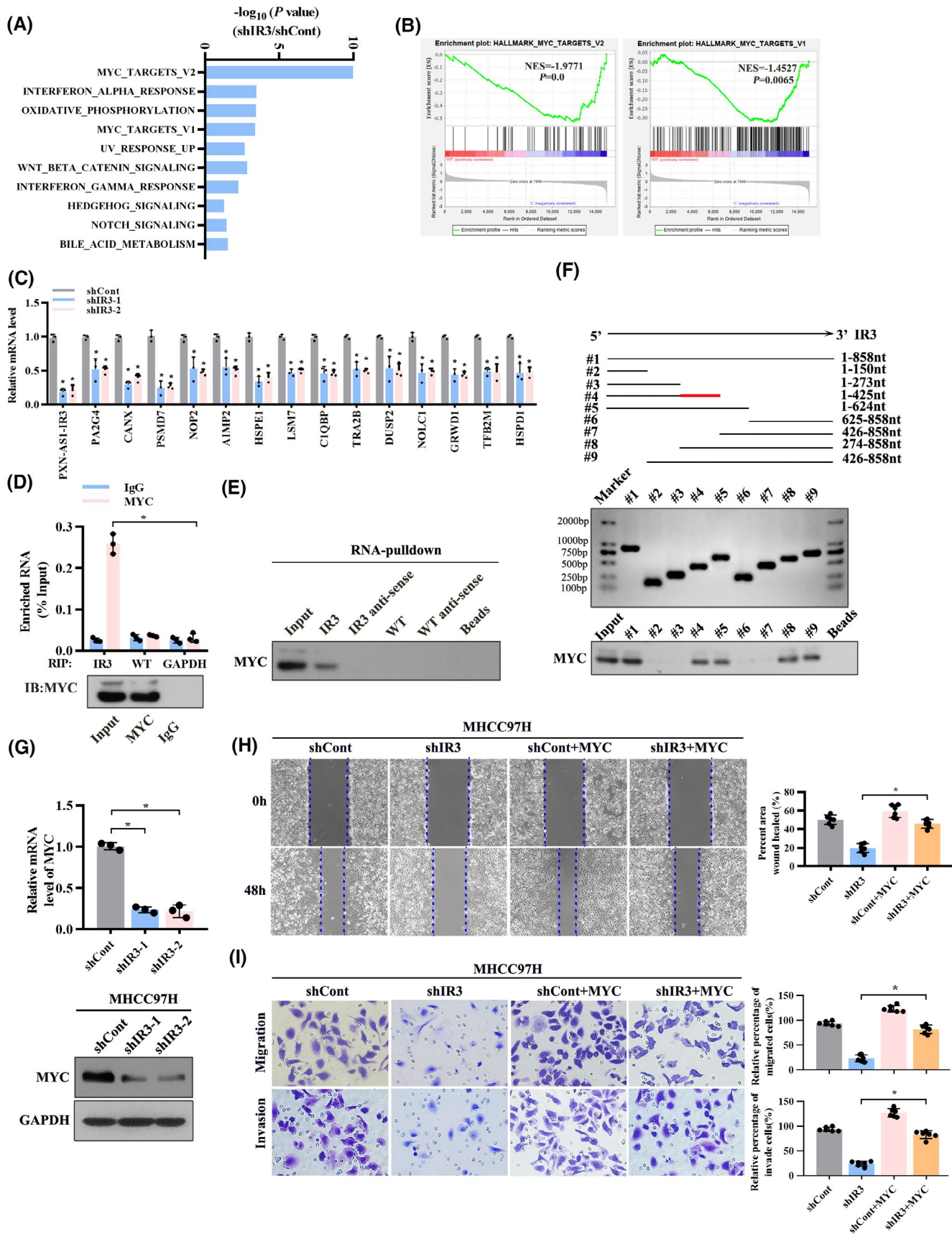
PXN-AS1-IR3 activates the MYC signaling pathway through chromatin modification of MYC enhancer

To explore the molecular mechanism underlying the oncogenic role of PXN-AS1-IR3 in HCC progression, we performed RNA-seq to identify downstream targets

in PXN-AS1-IR3 knockdown cells. We then performed gene-set enrichment analysis (GSEA) and found that multiple metastasis-related biological processes such as “MYC targets,” “Wnt pathway,” and “NOTCH signaling” were significantly deregulated by PXN-AS1-IR3 deficiency (Figure 6A). Among them, GSEA focused primarily on MYC signaling showed significant enrichment in PXN-AS1-IR3-silenced HCC cells (Figure 6B). To determine whether MYC signaling pathway was affected in the absence of PXN-AS1-IR3, several MYC targets, such as PA2G4, CANX, PSMD7, NOP2, AIMP2, HSPE1, LSM7, C1QBP, TRA2B, DUSP2, NOLC1, GRWD1, TFB2M and HSPD1, were significantly found down-regulated by PXN-AS1-IR3 knockdown, as evidenced by Real time PCR (Figure 6C). RNA immunoprecipitation assay further revealed that PXN-AS1-IR3, but not PXN-AS1-WT, was enriched by MYC RIP and RNA pull-down assay also confirmed the interaction between PXN-AS1-IR3 and MYC protein (Figure 6D,E). Furthermore, we performed RNA pull-down assays with a series of truncated fragments of PXN-AS1-IR3 and found that the 274–425-nt region of PXN-AS1-IR3 mediates the interaction with MYC (Figure 6F). This biological region (274–425-nt) is located exactly in the intron 3 (274–425-nt) of the PXN-AS1-IR3, suggesting that PXN-AS1-IR3, but not PXN-AS1-WT, specifically binds to MYC.

Moreover, PXN-AS1-IR3 knockdown resulted in decreased MYC mRNA and protein levels (Figure 6G). In contrast, PXN-AS1-IR3 overexpression resulted in opposite phenotypes (Figure S12A,B), suggesting that PXN-AS1-IR3 might regulate MYC expression at the transcriptional or post-transcriptional level. Next, we overexpressed MYC in PXN-AS1-IR3 knockdown cells or DDX17 knockout cells to explore whether the effect of DDX17 on HCC cells tumorigenesis was mediated by MYC. MYC overexpression significantly restored the migration and invasion ability of PXN-AS1-IR3 knockdown HCC cells (Figure 6H,I). Similarly, DDX17 knockout also led to a decrease of MYC mRNA and protein levels (Figure S12C,D). DDX17 knockout-induced inhibition of migration and invasion was blocked by MYC overexpression (Figure S12E,F). Collectively, these results suggest that MYC is involved in the DDX17-PXN-AS1-IR3 regulatory axis.

FIGURE 6 PXN-AS1-IR3 enhances MYC signaling in HCC. (A) RNA-seq was subjected to screen the downstream genes regulated by PXN-AS1-IR3, and the differential expression genes were analyzed by gene-set enrichment analysis (GSEA). The top 10 most-enriched gene sets are shown. (B) GSEA plots of “MYC target” pathway-related signatures in PXN-AS1-IR3-depleted cells versus control cells. (C) PXN-AS1-IR3-regulated genes involved in the MYC signaling pathway were confirmed by Real time PCR. * $p < 0.05$. (D) Enrichment of PXN-AS1-IR3 on MYC was detected by RIP assay (top). Western blot was performed to confirm that MYC was immunoprecipitated in the RIP experiments (bottom). (E) Specific associations of MYC protein with PXN-AS1-IR3, but not PXN-AS1-WT, were detected by RNA pull-down assay. (F) Schematic of truncated PXN-AS1-IR3 (top). The full-length PXN-AS1-IR3 (#1) and truncated PXN-AS1-IR3 (#2, 1-150 nt; #3, 1-273 nt; #4, 1-425 nt; #5, 1-624 nt; #6, 625-858 nt; #7, 426-858 nt; #8, 274-858 nt; #9, 426-858 nt) were confirmed by PCR (middle). The binding of MYC protein with truncated PXN-AS1-IR3 was detected by RNA pull-down assay (bottom). (G) Effect of PXN-AS1-IR3 knockdown on MYC mRNA and protein level was examined by Real time PCR and western blot, respectively. * $p < 0.05$. (H) Effect of MYC on healing velocity in PXN-AS1-IR3 knockdown cells was determined by wound healing assay. The distance was measured from six images. (I) Effect of MYC on HCC migration and invasion in PXN-AS1-IR3 knockdown cells was determined by transwell assay. * $p < 0.05$. IB, immunoblot; NES, normalized enrichment score



To investigate the molecular mechanism underlying PXN-AS1-IR3-regulated MYC expression, we first examined the effect of PXN-AS1-IR3 on the half-life of the MYC protein by using a cycloheximide chase assay. The half-life of the MYC protein was significantly increased by PXN-AS1-IR3 overexpression, suggesting that the interaction between PXN-AS1-IR3 and MYC help to increase protein stability of MYC (Figure S13A). Additionally, the subcellular fractions and immunofluorescence assays demonstrated that PXN-AS1-IR3 overexpression had no significant effect on nuclear-translocation of MYC (Figure S13B,C).

Next, to explore how PXN-AS1-IR3 regulates MYC transcription, we performed RNA pulldown assays and mass spectrometry to identify the proteins associated with PXN-AS1-IR3 (Figure 7A and Table S10). Among these proteins, we focused on the top 100 ranked protein testis expressed 10 (Tex10), which plays an important role in transcriptional regulation by modifying H3K4 methylation and recruiting the coactivator histone acetyltransferase p300. Interestingly, RNA pulldown assay and RIP assay confirmed the significant binding of PXN-AS1-IR3 to Tex10 protein, while only minimal binding with PXN-AS1-WT (Figure 7B,C). RNA pulldown assay showed that 274–624-nt fragment of PXN-AS1-IR3 was responsible for its association with Tex10 (Figure S14A). As expected, gene silencing of Tex10 suppressed MYC protein level (Figure 7D). Overexpression of Tex10 markedly blocked PXN-AS1-IR3 knockdown-induced inhibition of MYC protein (Figure 7E). These data suggested that Tex10 might play a major role in PXN-AS1-IR3-induced MYC expression, although PXN-AS1-IR3 enhanced MYC protein stability. To investigate whether PXN-AS1-IR3-mediated regulation of MYC was dependent on Tex10, we examined MYC expression in response to PXN-AS1-IR3 in Tex10-knockout cells. We found that IR3 overexpression in Tex10-knockout cells could not be efficiently increased MYC protein level (Figure S14B). These results indicate that PXN-AS1-IR3-induced regulation of MYC transcription is dependent on Tex10. Chromatin immunoprecipitation assay further revealed that PXN-AS1-IR3 knockdown substantially reduced the occupancy of Tex10 and p300 at the enhancer region of the MYC gene, while PXN-AS1-IR3 overexpression exhibited the opposite

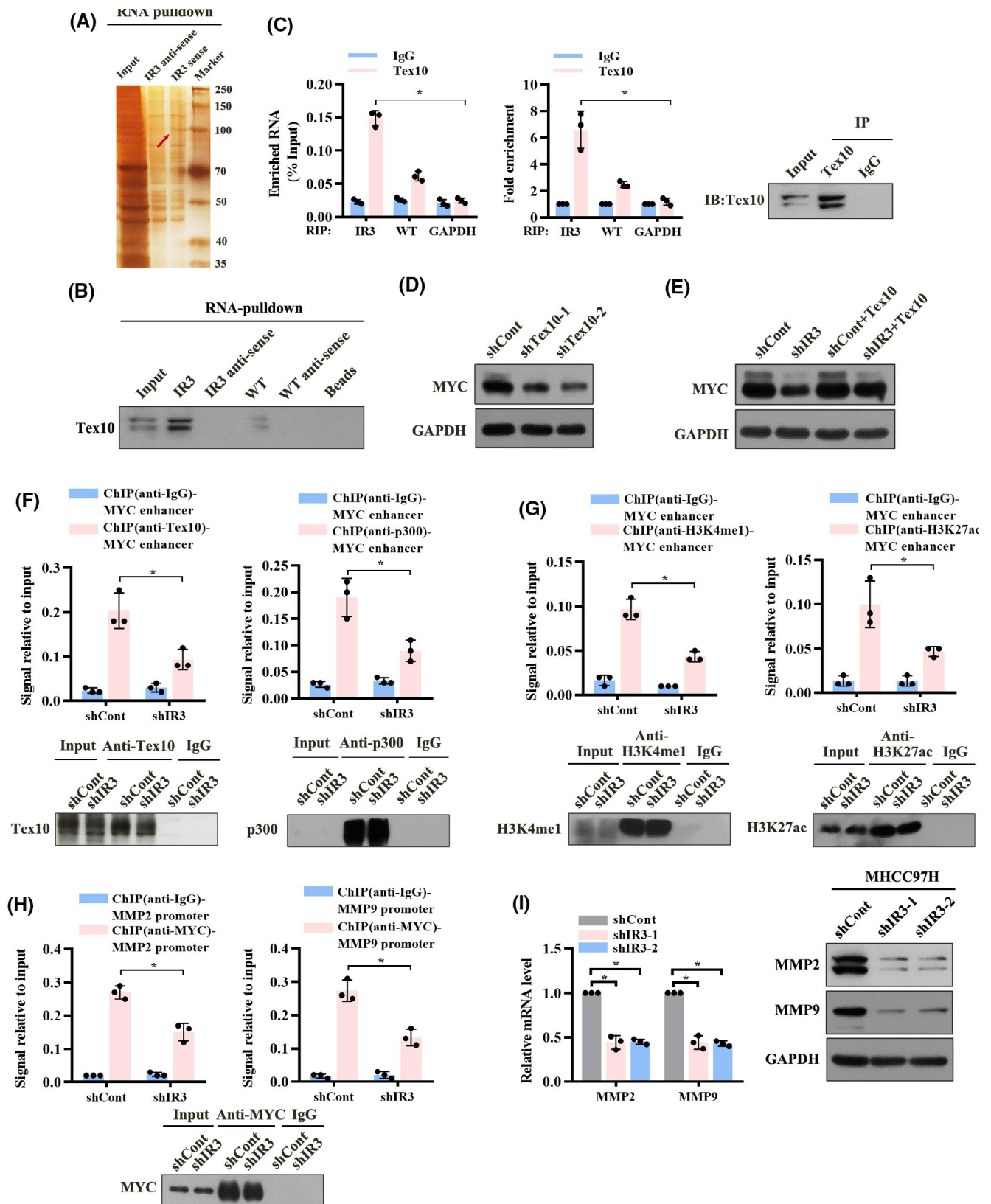
effect (Figures 7F and S15A). Consistently, PXN-AS1-IR3 knockdown resulted in decreased levels of active enhancer marks (H3K4me1 and H3K27ac) (Figure 7G). Consequently, PXN-AS1-IR3 knockdown caused decreased enrichment of MYC binding at the promoter regions of downstream genes MMP2 and MMP9, which finally led to decreased mRNA and protein levels of MMP2 and MMP9 (Figure 7H,I). Conversely, overexpression of PXN-AS1 in HCCLM3 cells increased the occupancy of MMP2 and MMP9 promoters by endogenous MYC (Figure S15B). These data suggest that PXN-AS1-IR3 promotes HCC progression by interacting with Tex10 to epigenetically regulate MYC expression.

Correlation among DDX17, PXN-AS1-IR3, and MYC expression in human HCC

To evaluate the clinical significance of PXN-AS1 in patients with HCC, we examined PXN-AS1-WT, PXN-AS1-IR3, and MYC mRNA levels in 84 pairs of primary HCC and adjacent nontumoral liver tissues, consisting of 56 pairs of MFH and 28 pairs of EHMH. The PXN-AS1-IR3 and MYC mRNA levels were significantly up-regulated in EHMH as compared with MFH, whereas the PXN-AS1-WT showed no significant change (Figure 8A). Correlative analysis showed that high PXN-AS1-IR3 mRNA level was correlated with AFP ($p = 0.0206$) and vascular invasion ($p = 0.0245$) (Table S11), whereas MYC mRNA level positively correlated with the tumor size ($p = 0.002$), tumor grade ($p = 0.0199$), and vascular invasion ($p = 0.0131$) (Table S12).

Moreover, we verified PXN-AS1-IR3 and PXN-AS1-WT levels in blood samples and HCC specimens in another HCC cohort with 40 pairs of EHMH and 40 pairs of MFH. The PXN-AS1-IR3 level, not PXN-AS1-WT, was significantly higher in serum and HCC tissues in EHMH group (Figure 8B,C). Correlative analysis revealed a positive correlation between *DDX17* and PXN-AS1-IR3, *DDX17* and *MYC*, and PXN-AS1-IR3 and *MYC* mRNA level in 40 pairs of EHMH (Figure 8D–F). Collectively, these data suggest that the DDX17-PXN-AS1-IR3-MYC regulatory axis may exist in vivo.

FIGURE 7 PXN-AS1-IR3 specifically binds to testis expressed 10 (Tex10). (A) Specific associations of proteins with biotinylated-PXN-AS1-IR3 were detected by streptavidin RNA pulldown assay and further analyzed by silver staining. The arrow indicates the PXN-AS1-IR3-specific band compared with antisense RNA. (B) Specific associations of Tex10 with PXN-AS1-IR3 and PXN-AS1-WT were detected by RNA pulldown assay. (C) Enrichment of PXN-AS1-IR3 and PXN-AS1-WT on Tex10 was detected by RIP assay. (D) Effect of Tex10 knockdown on MYC was examined by western blot. GAPDH was used as loading control. (E) Effect of MYC overexpression in Tex10 knockdown cells was examined by western blot. GAPDH were used as loading control. (F,G) Level of Tex10, p300, H3K4me1, and H3K27ac associated with MYC enhancer region in PXN-AS1-IR3 knockdown cells was examined by chromatin immunoprecipitation (ChIP) assay. Western blot was performed to confirm that Tex10, p300, H3K4me1, and H3K27ac were immunoprecipitated in the ChIP experiments. (H) Level of MYC associated with MMP2 promoter (left) and MMP9 promoter (right) in PXN-AS1-IR3 knockdown cells was examined by ChIP assay. Western blot was performed to confirm that MYC was immunoprecipitated in the ChIP experiments. (I) Effect of PXN-AS1-IR3 knockdown on MMP2 and MMP9 expression was examined by Real time PCR and western blot, respectively



DISCUSSION

Accumulating evidences have indicated that aberrant alternative splicing profile significantly increases the

complexity of the oncogenic network and contributes to cancer development and progression.^[6,22,23] In recent years, great achievements of the diversity of AS maps for HCC have been made due to the rapid development

of high-throughput sequencing technologies. Li et al. detected various differentially spliced ASEs in primary HCC tissues. It was pointed out that differential AS events participated in many cancer-related biological processes, and 243 differential ASEs were identified as risk predictors for survival of patients with HCC.^[24] Chen et al. have determined the tumor specificity of some AS variants including enzyme regulators (Rho/Rac Guanine Nucleotide Exchange Factor 2 [ARHGEF2], Serpin Family H Member 1 [SERPINH1]), chromatin modifiers (DEK Proto-Oncogene [DEK], Cyclin Dependent Kinase 9 [CDK9], RB Binding Protein 7 [RBBP7]), RNA-binding proteins (Serine And Arginine Rich Splicing Factor 3 [SRSF3], RNA Binding Motif Protein 27 [RBM27], Matrin 3 [MATR3], Y-Box Binding Protein 1 [YBX1]), and receptors (ADRM1 26S Proteasome Ubiquitin Receptor [ADRM1], Variant isoform of CD44 molecule [CD44v8-10], vitamin D receptor [VDR], Receptor Tyrosine Kinase Like Orphan Receptor 1 [ROR1]) in HCC tumors.^[25]

In addition to clinical samples originating from primary HCC and adjacent normal liver tissue used by most studies, we integrated primary HCC tissues with extrahepatic metastasis and metastasis-free HCC tissues in this study. So far, little is known about the transcriptome-wide landscape of AS events associated with HCC metastasis. In this study, we have obtained a comprehensive repertoire of AS events in HCC with extrahepatic metastasis and made several significant findings. First, we identified differentially 99,407 AS events in EHMH and 1070 differentially AS events involving 798 genes in EHMH compared with MFH, indicating that global splicing dysregulation augments occurred in HCC development and progression. Second, the 798 protein-coding genes that harbor differential AS events were highly enriched for the master regulator of metastasis-related signaling pathways, suggesting that splicing of these genes might represent an alternate mechanism for HCC metastasis. Third, 50% of differentially expressed metastasis-associated genes in EHMH have significant differentially AS events, suggesting that alternative splicing contributes to HCC development, at least in part, on expression alterations.

AS programs are largely controlled by a small number of master splicing regulators. Abnormal splicing regulators expression and/or activity often elicit changes in alternative splicing to promote oncogenic transformation.^[8] Some splicing regulators can act as oncoproteins when overexpressed in several tumors. SF2/ASF identified as a proto-oncogene was up-regulated in various human tumors, where it controls alternative splicing of the tumor suppressor Bridging Integrator 1 (BIN1) and the kinases MAPK Interacting Serine/Threonine Kinase 2 (MNK2) and Ribosomal Protein S6 Kinase B1 (S6K1).^[26,27] The splicing regulators of the SR and hnRNP families are overexpressed in multiple tumor

types and induce cancerogenesis-impaired apoptotic control through alternative splicing of some apoptotic genes.^[28] Conversely, down-regulation of splicing factors that act as tumor suppressors have been also reported. The STAR family protein quaking (QKI) was down-regulated in lung cancer, and its overexpression inhibits the proliferation of lung cancer cells by regulating the alternative splicing of NUMB Endocytic Adaptor Protein (NUMB).^[29] RBM4 is down-regulated in multiple cancers and has been characterized as a tumor suppressor that regulates BCL2 Like 1 (BCL2L1) splicing.^[30] In this study, DDX17 was identified as a proto-oncogene that was important for the aberrant AS and HCC metastasis. DDX17 was significantly up-regulated in EHMH and was strongly associated with outcome of patients with HCC. DDX17 knockout diminished the invasive ability of HCC cells, in part by regulating the alternative splicing of PXN-AS1, suggesting that DDX17 acts as a pro-tumorigenic splicing factor in HCC progression.

Recent studies have identified several downstream targets of DDX17 through alternative splicing in various types of cancer.^[13,15,31] It has been reported that DDX17 plays an important role in the alternative splicing on pre-mRNAs. DDX17 impacts on ER and AR protein stability in breast and prostate cancers by regulating alternative splicing of GSK3 β .^[31] Additionally, DDX17 promotes tumor cell invasiveness by regulating alternative splicing of chromatin-binding factors, macroH2A1 histone, or transcription factor NFAT5.^[13,14] However, DDX17-mediated regulation of alternative splicing on long non-coding RNAs has been rarely reported. Here, we systematically analyzed the DDX17-regulated alternative splicing events in HCC cells by combining the RNA-seq and RIP-seq data and finally focused on splicing of PXN-AS1. Many studies have linked the altered expression and/or variants of PXN-AS1 with tumor progression. PXN-AS1 suppresses pancreatic cancer progression by functioning as a competing sponge of miR-3064 to up-regulate the tumor suppressor PIP4K2B,^[32] suggesting that PXN-AS1 may be a tumor suppressor. However, PXN-AS1 expression has been up-regulated in a variety of cancers, including glioblastoma,^[33] nasopharyngeal carcinoma,^[34] non-small cell lung cancer,^[35] and liver cancer.^[36] Yuan et al. has reported that PXN-AS1 is subjected to skipping exon splicing and yields two isoforms, PXN-AS1 exon 4 inclusion and PXN-AS1 exon 4 skipping, which have an opposing role in HCC tumorigenesis.^[36] In this study, we identified a transcript PXN-AS1-IR3 with intron 3 retention that was produced in HCC cells and tissues with high DDX17. Furthermore, PXN-AS1-IR3 knockdown significantly decreased the migration and invasion activities of HCC cells in vitro and in vivo. These findings revealed that this transcript PXN-AS1-IR3 acts as an important oncogenic driver in the development and progression

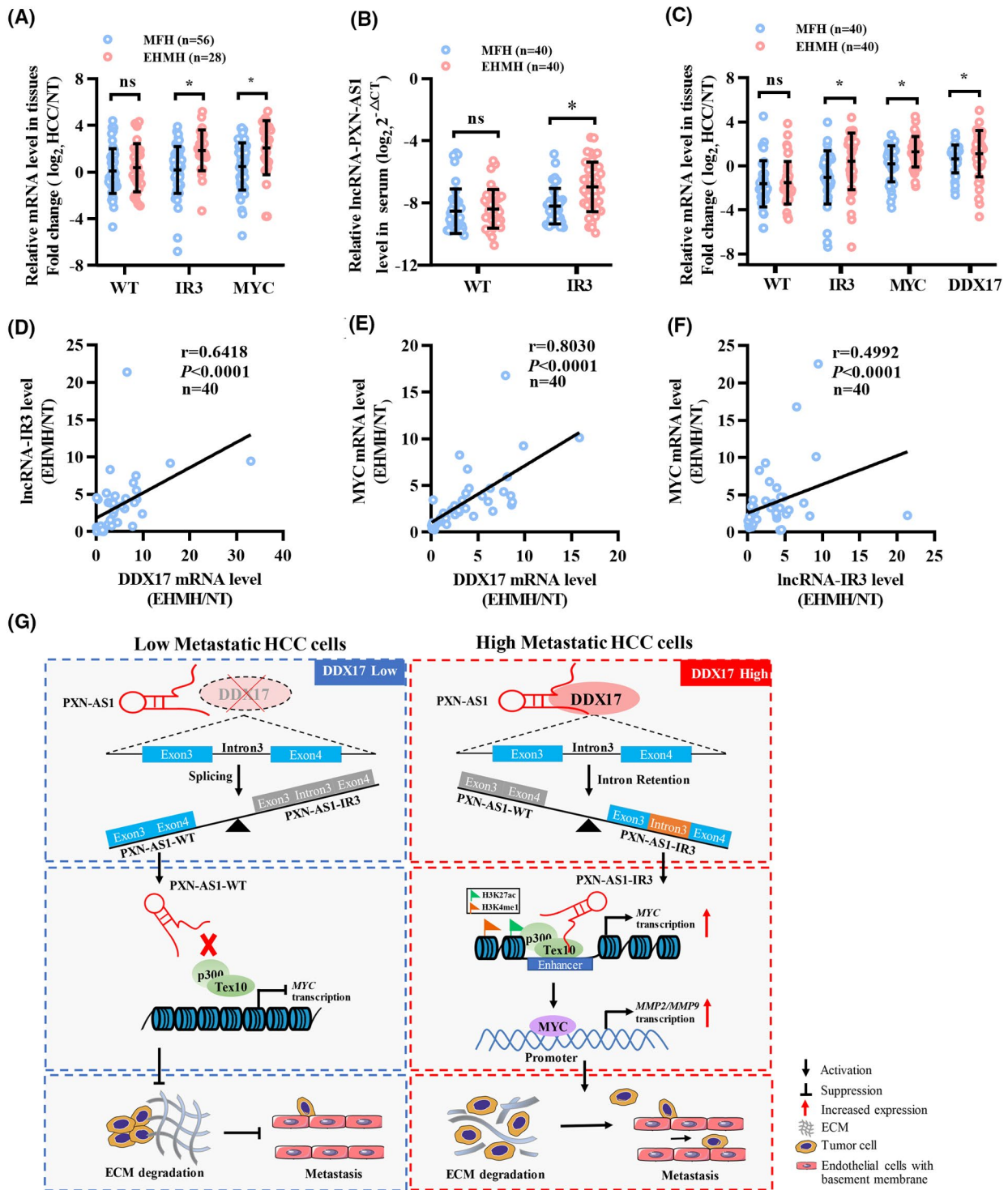


FIGURE 8 Correlation among DDX17, PXN-AS1-IR3, and MYC expression in HCC specimens. (A) The mRNA level of PXN-AS1-WT, PXN-AS1-IR3, and MYC in liver tissues from patients with HCC with MFH ($n = 56$) or EHMH ($n = 28$) was determined by Real time PCR. (B) Expression of PXN-AS1-WT and PXN-AS1-IR3 in the serum from patients with HCC with EHMH ($n = 40$) or MFH ($n = 40$) was determined by Real time PCR. (C) Expression of PXN-AS1-WT, PXN-AS1-IR3, MYC, and DDX17 in liver tissues from patients with HCC with EHMH ($n = 40$) or MFH ($n = 40$) was determined by Real time PCR. (D–F) Correlation between the mRNA level of DDX17 and PXN-AS1-IR3 ($n = 40$) (D), DDX17 and MYC ($n = 40$) (E), and PXN-AS1-IR3 and MYC ($n = 40$) (F) in EHMH tissues was analyzed by Spearman rank test. The expression of PXN-AS1-IR3, DDX17, and MYC mRNA level was normalized by GAPDH mRNA. (G) Mechanistic model of DDX17-mediated PXN-AS1 intron 3 retention to promote HCC migration. In low metastatic HCC cells, PXN-AS1-WT is the main isoform that had no significant effect on MYC expression or HCC migration (left). In high metastatic HCC cells, DDX17 expression level is obviously up-regulated, which led to PXN-AS1 intron 3 retention (PXN-AS1-IR3) (right). Up-regulated PXN-AS1-IR3 functions as a scaffold recruiting Tex10 and p300 to MYC enhancer. Activated MYC further enhance the expression of downstream genes including MMP2 and MMP9, and finally promote HCC metastasis. ECM, extracellular matrix; ns, not significant

of HCC. Moreover, PXN-AS1-IR3 overexpression remarkably restored the migration and invasion abilities of DDX17 knockout cells, suggesting that the alternative splicing of PXN-AS1 mediated, at least in part, the pro-metastatic function of DDX17. However, whether other DDX17-regulated AS events on pre-mRNA contribute to the pro-tumorigenic function of DDX17 is worth investigating further.

In summary, we have systematically analyzed alternative splicing events and splicing factors in HCC with metastasis and identified splicing regulator DDX17 as an oncoprotein, which was important for the aberrant AS and HCC metastasis. The splicing regulator DDX17 promotes HCC growth and metastasis by inducing intron 3 retention of PXN-AS1 to produce the transcript PXN-AS1-IR3. This transcript PXN-AS1-IR3 acts as an important oncogenic driver for HCC cell migration *in vitro* and *in vivo* by inducing transcriptional activation of MYC, which finally leads to the transcriptional activation of several metastasis-associated genes (Figure 8G). DDX17 and PXN-AS1-IR3 represent prognostic biomarkers and potential targets for the development of mechanism-based cancer prevention strategies.

CONFLICT OF INTEREST

The authors declare no potential conflicts of interest.

AUTHOR CONTRIBUTIONS

H.Z.Z., F.L., S.T.C., Y.X., H.J.D., Y.J.Z., M.L.Y. and J.H.R. performed the experiments and generated data. H.Z.Z., F.L., S.T.C., Y.X., H.J.D., D.Y.G., J.W., W.X.C., Y.J.Z., M.L.Y., J.H.R., L.Z., A.L.H. and J.C. analyzed the data. L.Z., A.L.H. and J.C. designed the experiments. H.Z.Z., F.L., S.T.C. and Y.X. wrote the manuscript. D.Y.G., J.W., W.X.C. and L.Z. provided clinical samples. All authors reviewed and approved the manuscript.

REFERENCES

- Villanueva A. Hepatocellular carcinoma. *N Engl J Med*. 2019;380:1450–62.
- Ryu SH, Jang MK, Kim WJ, Lee D, Chung YH. Metastatic tumor antigen in hepatocellular carcinoma: golden roads toward personalized medicine. *Cancer Metastasis Rev*. 2014;33:965–80.
- Lambert AW, Pattabiraman DR, Weinberg RA. Emerging biological principles of metastasis. *Cell*. 2017;168:670–91.
- Ule J, Blencowe BJ. Alternative splicing regulatory networks: functions, mechanisms, and evolution. *Mol Cell*. 2019;76:329–45.
- Bonnal SC, López-Oreja I, Valcárcel J. Roles and mechanisms of alternative splicing in cancer — implications for care. *Nat Rev Clin Oncol*. 2020;17:457–74. <http://dx.doi.org/10.1038/s41571-020-0350-x>
- Kahles A, Lehmann K-V, Toussaint NC, Hüser M, Stark S, Sachsenberg T, et al. Comprehensive Analysis of Alternative Splicing Across Tumors from 8,705 Patients. *Cancer Cell*. 2018;34:211–24.e6. <http://dx.doi.org/10.1016/j.ccell.2018.07.001>
- Hu X, Harvey SE, Zheng R, Lyu J, Grzeskowiak CL, Powell E, et al. The RNA-binding protein AKAP8 suppresses tumor metastasis by antagonizing EMT-associated alternative splicing. *Nat Commun*. 2020;11:486.
- Rahman MA, Krainer AR, Abdel-Wahab O. SnapShot: splicing alterations in cancer. *Cell*. 2020;180:208.e1. <http://dx.doi.org/10.1016/j.cell.2019.12.011>
- Linder P, Jankowsky E. From unwinding to clamping—the DEAD box RNA helicase family. *Nat Rev Mol Cell Biol*. 2011;12:505–16.
- Xue Y, Jia X, Li C, Zhang KE, Li L, Wu J, et al. DDX17 promotes hepatocellular carcinoma progression via inhibiting Klf4 transcriptional activity. *Cell Death Dis*. 2019;10:1–11.
- Sallam T, Jones M, Thomas BJ, Wu X, Gilliland T, Qian K, et al. Transcriptional regulation of macrophage cholesterol efflux and atherogenesis by a long noncoding RNA. *Nat Med*. 2018;24:304–12.
- Mori M, Triboulet R, Mohseni M, Schlegelmilch K, Shrestha K, Camargo FD, et al. Hippo signaling regulates microprocessor and links cell-density-dependent miRNA biogenesis to cancer. *Cell*. 2014;156:893–906.
- Dardenne E, Pierredon S, Driouch K, Gratadou L, Lacroix-Triki M, Espinoza MP, et al. Splicing switch of an epigenetic regulator by RNA helicases promotes tumor-cell invasiveness. *Nat Struct Mol Biol*. 2012;19:1139–46.
- Germann S, Gratadou L, Zonta E, Dardenne E, Gaudineau B, Fougère M, et al. Dual role of the ddx5/ddx17 RNA helicases in the control of the pro-migratory NFAT5 transcription factor. *Oncogene*. 2012;31:4536–49.
- Hönig A, Auboeuf D, Parker MM, O'Malley BW, Berget SM. Regulation of alternative splicing by the ATP-dependent DEAD-box RNA helicase p72. *Mol Cell Biol*. 2002;22:5698–707.
- Wang Z, Burge CB. Splicing regulation: from a parts list of regulatory elements to an integrated splicing code. *RNA*. 2008;14:802–13.
- Piva F, Giulietti M, Burini AB, Principato G. SpliceAid 2: a database of human splicing factors expression data and RNA target motifs. *Hum Mutat*. 2012;33:81–5.
- Ameur LB, Marie P, Thenoz M, Giraud G, Combe E, Claude J-B, et al. Intragenic recruitment of NF- κ B drives splicing modifications upon activation by the oncogene Tax of HTLV-1. *Nat Commun*. 2020;11:3045.
- Genov N, Basti A, Abreu M, Astaburuaga R, Relógio A. A bioinformatic analysis identifies circadian expression of splicing factors and time-dependent alternative splicing events in the HD-MY-Z cell line. *Sci Rep*. 2019;9:11062.
- Sveen A, Agesen TH, Nesbakken A, Rognum TO, Lothe RA, Skotheim RI. Transcriptome instability in colorectal cancer identified by exon microarray analyses: associations with splicing factor expression levels and patient survival. *Genome Med*. 2011;3:32.
- Sebestyén E, Singh B, Miñana B, Pagès A, Mateo F, Pujana MA, et al. Large-scale analysis of genome and transcriptome alterations in multiple tumors unveils novel cancer-relevant splicing networks. *Genome Res*. 2016;26:732–44.
- Climente-González H, Porta-Pardo E, Godzik A, Eyra E. The functional impact of alternative splicing in cancer. *Cell Rep*. 2017;20:2215–26.
- Montes M, Sanford BL, Comiskey DF, Chandler DS. RNA splicing and disease: animal models to therapies. *Trends Genet*. 2019;35:68–87.
- Li S, Hu Z, Zhao Y, Huang S, He X. Transcriptome-wide analysis reveals the landscape of aberrant alternative splicing events in liver cancer. *Hepatology*. 2019;69:359–75.
- Chen H, Gao F, He M, Ding XF, Wong AM, Sze SC, et al. Long-read RNA sequencing identifies alternative splice variants in hepatocellular carcinoma and tumor-specific isoforms. *Hepatology*. 2019;70:1011–25.
- Karni R, de Stanchina E, Lowe SW, Sinha R, Mu D, Krainer AR. The gene encoding the splicing factor SF2/ASF is a proto-oncogene. *Nat Struct Mol Biol*. 2007;14:185–93.

27. Ghigna C, Giordano S, Shen H, Benvenuto F, Castiglioni F, Comoglio PM, et al. Cell motility is controlled by SF2/ASF through alternative splicing of the Ron protooncogene. *Mol Cell*. 2005;20:881–90.
28. Kędzierska H, Piekietko-Witkowska A. Splicing factors of SR and hnRNP families as regulators of apoptosis in cancer. *Cancer Lett*. 2017;396:53–65.
29. Zong F-Y, Fu X, Wei W-J, Luo Y-G, Heiner M, Cao L-J, et al. The RNA-binding protein QKI suppresses cancer-associated aberrant splicing. *PLoS Genet*. 2014;10:e1004289.
30. Wang Y, Chen D, Qian H, Tsai Y, Shao S, Liu Q, et al. The splicing factor RBM4 controls apoptosis, proliferation, and migration to suppress tumor progression. *Cancer Cell*. 2014;26:374–89.
31. Samaan S, Tranchevent L-C, Dardenne E, Polay Espinoza M, Zonta E, Germann S, et al. The Ddx5 and Ddx17 RNA helicases are cornerstones in the complex regulatory array of steroid hormone-signaling pathways. *Nucleic Acids Res*. 2014;42:2197–207.
32. Yan J, Jia Y, Chen H, Chen W, Zhou X. Long non-coding RNA PXN-AS1 suppresses pancreatic cancer progression by acting as a competing endogenous RNA of miR-3064 to upregulate PIP4K2B expression. *J Exp Clin Cancer Res*. 2019;38:390.
33. Chen H, Hou G, Yang J, Chen W, Guo L, Mao Q, et al. SOX9-activated PXN-AS1 promotes the tumorigenesis of glioblastoma by EZH2-mediated methylation of DKK1. *J Cell Mol Med*. 2020;24:6070–82.
34. Jia X, Niu P, Xie C, Liu H. Long noncoding RNA PXN-AS1-L promotes the malignancy of nasopharyngeal carcinoma cells via upregulation of SAPCD2. *Cancer Med*. 2019;8:4278–91.
35. Zhang Z, Peng Z, Cao J, Wang J, Hao Y, Song K, et al. Long noncoding RNA PXN-AS1-L promotes non-small cell lung cancer progression via regulating PXN. *Cancer Cell Int*. 2019;19:20.
36. Yuan J-h, Liu X-n, Wang T-t, Pan W, Tao Q-f, Zhou W-p, et al. The MBNL3 splicing factor promotes hepatocellular carcinoma by increasing PXN expression through the alternative splicing of lncRNA-PXN-AS1. *Nat Cell Biol*. 2017;19:820–32.

SUPPORTING INFORMATION

Additional supporting information may be found in the online version of the article at the publisher's website.

How to cite this article: Zhou H-Z, Li F, Cheng S-T, Xu Y, Deng H-J, Gu D-Y, et al. DDX17-regulated alternative splicing that produced an oncogenic isoform of PXN-AS1 to promote HCC metastasis. *Hepatology*. 2022;75:847–865. <https://doi.org/10.1002/hep.32195>